

IMAGE FORGERY LOCALIZATION BASED ON MULTI-SCALE CONVOLUTIONAL NEURAL NETWORKS

Yaqi Liu, Qingxiao Guan, Xianfeng Zhao, and Yun Cao

1. State Key Laboratory of Information Security, Institute of Information Engineering, Chinese Academy of Sciences, Beijing 100093, China
2. School of Cyber Security, University of Chinese Academy of Sciences, Beijing 100093, China

ABSTRACT

In this paper, we propose to utilize Convolutional Neural Networks (CNNs) and the segmentation-based multi-scale analysis to locate tampered areas in digital images. First, to deal with color input sliding windows of different scales, a unified CNN architecture is designed. Then, we elaborately design the training procedures of CNNs on sampled training patches. With a set of robust multi-scale tampering detectors based on CNNs, complementary tampering possibility maps can be generated. Last but not least, a segmentation-based method is proposed to fuse the maps and generate the final decision map. By exploiting the benefits of both the small-scale and large-scale analyses, the segmentation-based multi-scale analysis can lead to a performance leap in forgery localization of CNNs. Numerous experiments are conducted to demonstrate the effectiveness and efficiency of our method.

Index Terms— Image forensics, forgery localization, multi-scale analysis, Convolutional Neural Networks.

1. INTRODUCTION

Image forgery localization is one of the most challenging tasks in digital image forensics [1]. Different from forgery detection which simply discriminates whether a given image is pristine or fake, image forgery localization attempts to detect the accurate tampered areas [2]. Since forgery localization needs to conduct pixel-level analyses, it is more difficult than the conventional forgery detection task.

Different clues are investigated to locate the tampered areas, e.g., the photo-response nonuniformity noise (PRNU) [3], the artifacts of Color Filter Array [4], the traces left by JPEG coding [5], the near-duplicate image analysis [6], and copy-move forgery detection [7], etc. The tampering operations inevitably distort some inherent relationships among the adjacent pixels, features motivated by steganalysis [8] are frequently adopted to localize tampered areas [9, 1]. In 2013,

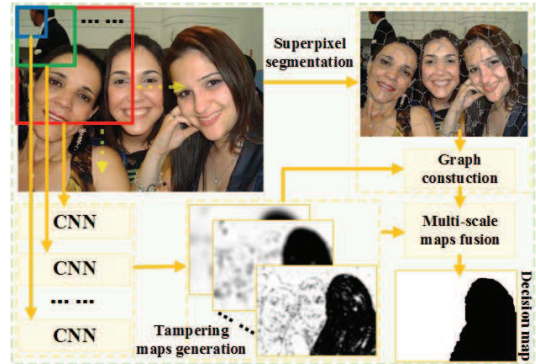


Fig. 1. The framework of the proposed forgery localization method based on Multi-Scale Convolutional Neural Networks (MSCNNs). Note that the sliding windows (blue, green, red squares) and superpixels do not indicate their real sizes.

IEEE Information Forensics and Security Technical Committee (IFS-TC) established the First IFS-TC Image Forensics Challenge [10]. In the second phase, a complicated and practical situation for evaluating the performance of forgery localization was set up. The winner [11] and successors [6, 1] combined different clues (all made use of copy-move clues) to achieve high scores. The best F1-score using a single clue for splicing detection (not specially for copy-move forgery detection) was achieved in [1] which was based on color rich models and the ensemble classifier (SCRM+LDA).

In this paper, we focus on forgery localization utilizing features extracted by Convolutional Neural Networks (CNNs) [12]. Booming in computer vision tasks, CNNs are also applied in image forensics. In [13], CNNs are applied in median filtering image forensics. In [14], a new form of convolutional layer is utilized to suppress the content of the image, and CNNs are adopted to detect multiple image manipulations. In [15], a CNN with SRM kernels [8] for the first layer initialization is adopted for forgery detection. More recently, [16] shows that residual-based descriptors can be regarded as a simple constrained CNN which can conduct forgery detection and localization.

This work was supported by the NSFC under U1536105 and U1636102, and National Key Technology R&D Program under 2014BAH41B01, 2016YFB0801003 and 2016QY15Z2500.

In this paper, an image forgery localization method based on Multi-Scale Convolutional Neural Networks (MSCNNs) is proposed, as shown in Fig. 1. In our method, sliding windows of different scales are put into a set of carefully designed and trained CNNs to generate real-valued tampering possibility maps. Then, based on the graph constructed on super-pixels [17], we can generate the final decision map by fusing those possibility maps. The contributions are two-fold: First, a unified CNN architecture is formulated for color patches, and multi-scale CNNs are treated as a set of “weak” classifiers to fully exploit the benefits of both the small-scale and large-scale analyses. Second, the segmentation-based fusion method is proposed to efficiently process images of different scales. On the IFS-TC dataset, MSCNNs can achieve the best performance utilizing the clue for splicing detection.

The rest of the paper is structured as follows. In Section 2, we introduce the architecture of CNNs and the training procedures. In Section 3, we introduce the generation and fusion of tampering possibility maps for MSCNNs. In Section 4, experiments are conducted. In Section 5, we draw conclusions.

2. CNNs FOR IMAGE FORGERY LOCALIZATION

Our motivation is that we want to replace the SCRM+LDA [1] with the end-to-end CNNs to estimate the tampering probability of a given patch. Adopting the sliding window manner, we can give the tampering possibility map of the investigated image. The CNNs proposed in [18] achieve the state-of-the-art performance for steganalysis on gray-scale images. In the first layer of their CNNs, a single high pass filter (we call it the base filter) is utilized to suppress the image content. In our work, to deal with color patches, two different kinds of base filters are tested: (1) Fixed SRM kernels: The base filters are fixed, and set as the SRM kernels [8]. All the kernels in [8] are adopted, and we leave the task of validating their effectiveness to the backend network. The 30 different kernels are formulated as 5×5 matrixes $\{\mathbf{F}_1, \dots, \mathbf{F}_{30}\}$ with zero-valued unused elements. The inputs are three-channel color patches, so we need 30×3 filters to generate 30 feature maps. For the j th feature map ($j \in \{1, 2, \dots, 30\}$), the corresponding filters are set as $\{\mathbf{F}_1^j, \mathbf{F}_2^j, \mathbf{F}_3^j\} = \{\mathbf{F}_{3k-2}, \mathbf{F}_{3k-1}, \mathbf{F}_{3k}\}$, where $k = ((j-1) \bmod 10) + 1$. (2) Constrained filters: in [14, 19], a kind of constrained filters are proposed for manipulation detection. Here, we adopt it for forgery localization. The constraint means that the filter weight at the center $f(0, 0) = -1$, and $\sum_{r,c \neq 0} f(r, c) = 1$, $f(r, c)$ denotes the element in the base filter \mathbf{F} . For fair comparisons, 90 5×5 constrained filters are adopted. As we adopt 90 base filters, we modulate the parameters of CNNs in [18], and the unified CNN architecture can be depicted as Fig. 2. For different scales of input patches, we only need to change P in the last average pooling layer, ensuring that the input of the fully-connected layer is a 256-dimensional vector. Note that the input patches for the CNNs should all subtract the mean values of each channel.

Table 1. The numbers of sampled patches on the IFS-TC.

Patch size	32	48	64	96	128
Training set	275046	309690	325942	339396	341930
Validation set	53938	61770	65704	68776	69044

There are 450 images in the training set of IFS-TC [10] with corresponding human-labeled ground truths. We randomly select 368 images for training and 75 images for validation (7 images are deserted for imperfect ground truths). Then, we sample patches on the images for training and validation. The sliding window size is $s \times s$, and in our work $s \in \{32, 48, 64, 96, 128\}$. During the patches generation, we also adopt the sliding window manner. The sliding window with a fixed scale slides across the full image. We set the stride st as 8 to get plenty of sampled patches. The patches tampered with 10% to 90% (discriminative features mostly appear around the contours of manipulated regions) are regarded as fake patches. The rates of the tampered areas in the full images differ greatly. In some images, more than ten thousand patches can be generated, while in some images, no patch can be generated with $st = 8$. The imbalance of patches distribution can lead to overfitting. So we set an upper threshold T for patches sampling. While more than T patches are generated, we randomly select T patches (we set $T = 500$ to make sure that we sample a similar number of patches on most images). With the sliding window sample manner, no patch can be generated for some images. For those images, we re-sample patches which are centered at the tampered areas. If the tampered rates of patches are satisfied, the patches are selected. After the fake patches are generated, we sample the same number of pristine patches in the same images, and the pristine patches do not have any tampered pixels. The numbers of patches we have sampled on the training set and validation set of IFS-TC are shown in TABLE 1. With 5 groups of patches for training and validation, 5 independent CNNs can be trained with patches of different scales as the inputs.

3. MAPS GENERATION AND FUSION

For each input image, it is analysed by the sliding window of the scale as $s \times s$ with a stride of st . Then, we can get the tampering possibility map $\hat{\mathbf{M}}_s$ of size $h_s \times w_s$, where $h_s = \lfloor (h-s)/st \rfloor + 1$ and $w_s = \lfloor (w-s)/st \rfloor + 1$, h and w denote the height and width of the input image, and $\lfloor \cdot \rfloor$ denotes the floor function. The elements in $\hat{\mathbf{M}}_s$ denote the probabilities of the corresponding patches being fake or pristine. We adopt the pristine probabilities, and a lower probability means that it is more likely to be fake. In order to get the possibility map \mathbf{M}_s with the same size as the input image, the element $m_{i,j}^s$ in \mathbf{M}_s is computed as:

$$m_{i,j}^s = \frac{1}{K} \sum_{k=1}^K \hat{m}_k^s \quad (1)$$

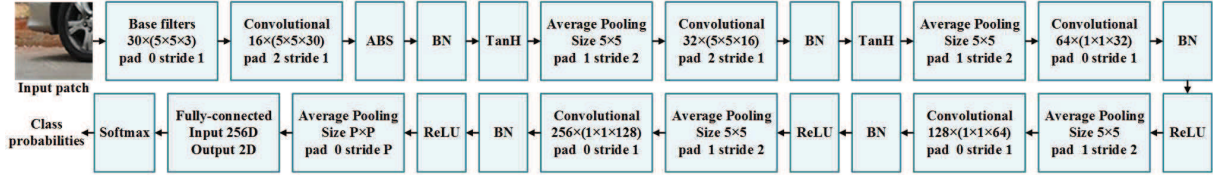


Fig. 2. The architecture and parameters of the unified Convolutional Neural Networks.

where K is the number of patches containing pixel $I_{i,j}$, and \hat{m}_k^s denotes the corresponding value in $\hat{\mathbf{M}}_s$. Inevitably, for some pixels, K is equal to 0, and the pixels always appear around the edges of the image. We simply set the same probabilities as the nearest pixels whose $K \neq 0$. Since we have a large stride st , there are mosaic artifacts in the possibility map generated by formula (1). To smooth the possibility map, the mean filtering is applied as:

$$\bar{m}_{i,j}^s = \frac{1}{s \times s} \sum_{i'=-\frac{s}{2}}^{\frac{s}{2}-1} \sum_{j'=-\frac{s}{2}}^{\frac{s}{2}-1} m_{i+i',j+j'}^s \quad (2)$$

where s denotes the size of corresponding patches. So that we can get the smoothed possibility map $\bar{\mathbf{M}}_s$.

With the analyses of multi-scale CNNs detectors, we can get a set of tampering possibility maps $\{\bar{\mathbf{M}}_s\}$ for each image, and $s \in \{32, 48, 64, 96, 128\}$ in our work. The final task is to fuse possibility maps to exploit the benefits of multi-scale analyses. In [2], the multi-scale analysis in PRNU-based tampering localization was proposed. By minimizing an energy function, tampering possibility maps fusion is formulated as a random-field problem where decision fusion resolves to finding an optimal labeling of authentication units. The optimization is conducted on the pixel level which takes too much time when there are more than 10^6 pixels in one image. Let alone, there are many images larger than 10^7 pixels in real life and the IFS-TC dataset. So we propose to construct graphs on superpixels and find the optimal labels on the superpixel level.

Simple linear iterative clustering (SLIC) [17] is a kind of commonly used efficient superpixel segmentation method, and we adopt SLIC to conduct oversegmentation on the investigated color images. In the computer vision tasks, images are usually segmented into hundreds of superpixels. However, in the task of tampering possibility maps fusion, large superpixels can lead to information loss. Thus, thousands of superpixels must be generated in our task. In [2], the optimization problem is solved by graph cut algorithm whose worst case running time complexity is $O(ev^2)$ [20], where v is the number of nodes in the graph and e is the edge number. And they consider a 2nd-order neighborhood, which means that $e \approx 4v$, so the complexity of the method is $O(v^3)$. They adopt pixels as the nodes in the graph, thus the computing time of the large image is almost unacceptable. While the complexity of SLIC is linear, i.e. $O(v)$, and it is easy to generate superpixels by SLIC for large images. Then, a graph on

the superpixels is constructed, each superpixel is treated as a node in the graph and the adjacent superpixels are connected by an edge. As above-mentioned, the number of superpixels is around several thousand, which is much easier to compute by graph cut. As for the superpixel-level tampering possibility maps generation, two strategies are tested. The one is “mean”, and the tampering possibility $m_{sup_l}^s$ of superpixel l under scale s is computed as:

$$m_{sup_l}^s = \frac{1}{P_l} \sum_{p=1}^{P_l} \bar{m}_p^s \quad (3)$$

where P_l denotes the number of pixels in superpixel l . \bar{m}_p^s is the element in $\bar{\mathbf{M}}_s$. The other strategy called “maxa” is:

$$m_{sup_l}^s = \bar{m}_{p_0}^s, p_0 = \arg \max_{p=1, \dots, P_l} (\text{abs}(\bar{m}_p^s - \theta)) \quad (4)$$

For $\bar{m}_p^s \in [0, 1]$, so we set $\theta = 0.5$. With the superpixel-level graph and superpixel-level tampering possibility maps at hands, it is easy to fuse the maps by minimizing the energy function in [2].

4. EXPERIMENTAL EVALUATION

The image corpus provided in the IFS-TC Image Forensics Challenge are adopted for evaluation. As above mentioned, there are 75 images for validation, and 700 testing images. We summarize localization performance as an average F1-score. The F1-scores on the testing images are computed by the evaluation system of the challenge [10]. Our method is implemented via Caffe and Matlab. Minibatch gradient descent is adopted for training, the momentum is 0.99 and weight decay is 0.0005. The learning rate is initialized to 0.001 and scheduled to decrease 10% for every 8000 iterations. The convolution kernels are initialized by random numbers generated from zero-mean Gaussian distribution with standard deviation of 0.01, and bias learning is disabled. The parameters in the fully-connected layer are initialized using “Xavier”. For different scales of patches, the sizes of the minibatches are set as $\{960, 960, 640, 480, 320\}$ corresponding to $s \in \{32, 48, 64, 96, 128\}$ (The minibatch sizes are modulated to make the most of our GPU memory). The caffemodels after 20000 iterations are adopted for all the scales.

As shown in TABLE 2, a comprehensive comparison between SCRM+LDA and different variants of CNNs is con-

Table 2. The comparison between SCRM+LDA and CNN on the IFS-TC validation set. Time-1 denotes the training time, and Time-2 denotes the average computing time.

Method	Size	Stride	Time-1 (s)	Time-2 (s)	F1-score
SCRM+LDA	64	16	3.20×10^5	2854.75	0.2847
SCRM+LDA+MF	64	16		2855.05	0.3123
CNN-SRM	64	16	3376.07	8.20	0.3285
CNN-SRM+MF	64	16		8.38	0.3354
CNN-SRM	64	8		17.11	0.3263
CNN-SRM+MF	64	8		17.32	0.3423
CNN-C-SRM+MF	64	8	3843.03	31.66	0.2816
CNN-C-GAU+MF	64	8	3849.09	31.71	0.2718

Table 3. F1-scores on the IFS-TC validation set.

	32	48	64	96	128
CNN-SRM	0.3028	0.3045	0.3263	0.3298	0.2817
CNN-SRM+MF	0.3285	0.3241	0.3423	0.3465	0.2888
MSCNNs-mean	0.3993				
MSCNNs-maxa	0.4028				

ducted. “MF” denotes mean filtering, and it can certainly improve the F1-scores based on the experimental observation. The training procedure of SCRM+LDA takes too much time. Although we have a powerful CPU, it takes almost 4 days. Furthermore, its average computing time on the images is also unacceptable. With the same patch size (64) and stride (16), the computing time of CNNs is $1/340$ of SCRM+LDA. CNN-SRM denotes the CNNs with fixed SRM base filters, CNN-C-SRM denotes constrained filters with SRM initialization and the base filters of CNN-C-GAU are constrained filters with gaussian initialization. It can be seen that CNN-SRM can achieve higher F1-scores. Because there are many zero values in the SRM base filters, it is also efficient than CNN-C-SRM and CNN-C-GAU.

For the good performance of CNN-SRM, we adopt this form of CNNs for multi-scale analyses, and the stride is set as 8. As shown in TABLE 4, CNNs with scales as 64 and 96 can achieve higher scores. Although no single-scale CNNs can achieve a score higher than 0.35, the multi-scale analysis can improve the performance significantly. “mean” and “maxa” represent the two strategies for superpixel-level tampering possibility maps generation. MSCNNs-maxa can achieve a higher score. All the images are empirically segmented into 4000 superpixels, and adaptive segmentation strategies for maps fusion need further research in the future.

Subsequently, we adopt five single-scale CNNs with the mean filtering and MSCNNs with two strategies to test on the testing images. As shown in TABLE 4, the left side presents the results of different variants of our method, and the right side presents results of the state-of-the-art methods for splicing detection. In another word, the compared methods are not designed for some particular cases, e.g. copy-move forgery detection, and can be utilized to detect any splicing forgeries. Their results are borrowed from their papers [1, 6, 11].

Table 4. Results on the IFS-TC testing set.

Variant	F1-score	Method	F1-score
32MF	0.3436	SCRM+LDA [1]	0.3458
48MF	0.3526	PRNU [6]	0.2535
64MF	0.3570	S3+LDA [1]	0.1737
96MF	0.3423	S3+SVM [11]	0.1115
128MF	0.3135		
MSCNNs-mean	0.4025		
MSCNNs-maxa	0.4063		

Table 5. Computing time on the IFS-TC testing set.

		32	48	64	96	128
CNNs	Average time (s)	15.47	15.10	17.74	19.21	19.56
	Median time (s)	7.96	7.67	8.89	9.33	9.20
MF	Average time (s)	0.08	0.13	0.19	0.37	0.63
	Median time (s)	0.04	0.07	0.11	0.20	0.35
Fusion	Average time (s)	20.88				
	Median time (s)	11.75				

SCRM+LDA adopts the sliding window manner with the scale of 64, and our CNN with $s = 64$ can achieve better performance than SCRM+LDA. Multi-scale analyses can greatly improve the performance of CNNs, and MSCNNs-maxa can achieve the similar F1-scores as the winner of IFS-TC challenge [11] which makes use of three different clues. While MSCNNs-maxa only utilize features extracted by CNNs and can be further improved by combining other clues.

We evaluate the computing time on the 700 testing images of IFS-TC whose sizes vary from 922×691 to 4752×3168 (most images are around 1024×768). We report the average time and median time for each step. Experiments are conducted on a machine with Intel(R) Core(TM) i7-5930K CPU @ 3.50GHz, 64GB RAM and a single GPU (TITAN X). As shown in TABLE 5, the computing time of 5-scales MSCNNs is around 60 s for most images. Furthermore, the MF and Fusion (including SLIC) procedures are implemented on CPU which can be further accelerated by implementing on GPU.

5. CONCLUSIONS

In this paper, a novel forgery localization method based on Multi-Scale Convolutional Neural Networks is proposed. CNNs for input patches of different scales are well designed and trained as a set of forgery detectors. Then, segmentation-based multi-scale analysis is utilized to dig out the information given by the different-scales analyses. Full experiments on the IFS-TC dataset demonstrate the effectiveness and efficiency of the proposed method named MSCNNs.

In the future work, the performance of CNNs can be improved by further elaborate design, and training on other datasets may also improve the robustness of the CNNs detectors. The existing works on IFS-TC only consider images without post compression, the robustness of the method against JPEG compression will also be studied, and eval-

uation on more extensive datasets will be conducted in the future.

6. REFERENCES

- [1] Haodong Li, Weiqi Luo, Xiaoqing Qiu, and Jiwu Huang, "Image forgery localization via integrating tampering possibility maps," *IEEE Transactions on Information Forensics and Security*, vol. 12, no. 5, pp. 1240–1252, 2017.
- [2] Paweł Korus and Jiwu Huang, "Multi-scale analysis strategies in prnu-based tampering localization," *IEEE Transactions on Information Forensics and Security*, vol. 12, no. 4, pp. 809–824, 2017.
- [3] Mo Chen, Jessica Fridrich, Miroslav Goljan, and Jan Lukás, "Determining image origin and integrity using sensor noise," *IEEE Transactions on Information Forensics and Security*, vol. 3, no. 1, pp. 74–90, 2008.
- [4] Pasquale Ferrara, Tiziano Bianchi, Alessia De Rosa, and Alessandro Piva, "Image forgery localization via fine-grained analysis of cfa artifacts," *IEEE Transactions on Information Forensics and Security*, vol. 7, no. 5, pp. 1566–1577, 2012.
- [5] Tiziano Bianchi and Alessandro Piva, "Image forgery localization via block-grained analysis of jpeg artifacts," *IEEE Transactions on Information Forensics and Security*, vol. 7, no. 3, pp. 1003–1017, 2012.
- [6] Lorenzo Gaborini, Paolo Bestagini, Simone Milani, Marco Tagliasacchi, and Stefano Tubaro, "Multi-clue image tampering localization," in *Information Forensics and Security (WIFS), 2014 IEEE International Workshop on*. IEEE, 2014, pp. 125–130.
- [7] Davide Cozzolino, Giovanni Poggi, and Luisa Verdoliva, "Efficient dense-field copy-move forgery detection," *IEEE Transactions on Information Forensics and Security*, vol. 10, no. 11, pp. 2284–2297, 2015.
- [8] Jessica Fridrich and Jan Kodovsky, "Rich models for steganalysis of digital images," *IEEE Transactions on Information Forensics and Security*, vol. 7, no. 3, pp. 868–882, 2012.
- [9] Davide Cozzolino and Luisa Verdoliva, "Single-image splicing localization through autoencoder-based anomaly detection," in *Information Forensics and Security (WIFS), 2016 IEEE International Workshop on*. IEEE, 2016, pp. 1–6.
- [10] "The first ieee ifs-tc image forensics challenge," <http://ifc.recod.ic.unicamp.br/fc.website/index.py>.
- [11] Davide Cozzolino, Diego Gragnaniello, and Luisa Verdoliva, "Image forgery localization through the fusion of camera-based, feature-based and pixel-based techniques," in *Image Processing (ICIP), 2014 IEEE International Conference on*. IEEE, 2014, pp. 5302–5306.
- [12] Alex Krizhevsky, Ilya Sutskever, and Geoffrey E Hinton, "Imagenet classification with deep convolutional neural networks," in *Advances in neural information processing systems*, 2012, pp. 1097–1105.
- [13] Jiansheng Chen, Xiangui Kang, Ye Liu, and Z Jane Wang, "Median filtering forensics based on convolutional neural networks," *IEEE Signal Processing Letters*, vol. 22, no. 11, pp. 1849–1853, 2015.
- [14] Belhassen Bayar and Matthew C Stamm, "A deep learning approach to universal image manipulation detection using a new convolutional layer," in *Proceedings of the 4th ACM Workshop on Information Hiding and Multimedia Security*. ACM, 2016, pp. 5–10.
- [15] Yuan Rao and Jiangqun Ni, "A deep learning approach to detection of splicing and copy-move forgeries in images," in *Information Forensics and Security (WIFS), 2016 IEEE International Workshop on*. IEEE, 2016, pp. 1–6.
- [16] Davide Cozzolino, Giovanni Poggi, and Luisa Verdoliva, "Recasting residual-based local descriptors as convolutional neural networks: an application to image forgery detection," *arXiv preprint arXiv:1703.04615*, 2017.
- [17] Radhakrishna Achanta, Appu Shaji, Kevin Smith, Aurelien Lucchi, Pascal Fua, and Sabine Süsstrunk, "Slic superpixels compared to state-of-the-art superpixel methods," *IEEE transactions on pattern analysis and machine intelligence*, vol. 34, no. 11, pp. 2274–2282, 2012.
- [18] Guanshuo Xu, Han-Zhou Wu, and Yun-Qing Shi, "Structural design of convolutional neural networks for steganalysis," *IEEE Signal Processing Letters*, vol. 23, no. 5, pp. 708–712, 2016.
- [19] Belhassen Bayar and Matthew C Stamm, "On the robustness of constrained convolutional neural networks to jpeg post-compression for image resampling detection," in *Acoustics, Speech and Signal Processing (ICASSP), 2017 IEEE International Conference on*. IEEE, 2017, pp. 2152–2156.
- [20] Yuri Boykov and Vladimir Kolmogorov, "An experimental comparison of min-cut/max-flow algorithms for energy minimization in vision," *IEEE transactions on pattern analysis and machine intelligence*, vol. 26, no. 9, pp. 1124–1137, 2004.